Control Performance Simulation in the Design of a Flapping Wing Micro-Aerial Vehicle

Lindsey L. Hines, Veaceslav Arabagi, and Metin Sitti, *Senior Member, IEEE*

Abstract— **Flapping wing micro-aerial vehicles (MAVs) hold great potential for matching the agility of flies, their source of inspiration. At small scales, however, it becomes difficult to balance design mechanical complexity and the weight/lift ratio. Considering control in the initial stages of vehicle design can help define system feasibility and the consequences of making design simplifications. Here, four design alternatives based on a piezoelectric driven passive pitch reversal wing are modeled and compared based on their performance under an ideal linear quadratic regulator (LQR) control scheme. State error over straight line, circular, and cube trajectories are used as a means of comparison. Wing lift and reasonable control input bounds are defined for each design variation. While not nearly as maneuverable as flies, these designs show promise as feasible controllable vehicles.**

I. INTRODUCTION

WHILE flies and their acrobatic maneuvers have long been a source of inspiration for aerial robotic platform development, reproducing their maneuverability in a Micro-Aerial Vehicle (MAV) at their size scale is quite difficult. On such weight limited platforms, one encounters a tradeoff between producing enough lift for liftoff yet designing the vehicle to be controllable in free flight. Adding additional controllable degrees of freedom greatly aids the controllability of the vehicle, at the cost of increased vehicle mass and manufacturing complexity. There have been multiple approaches pursued in the development of MAVs, from motor based four winged vehicles, such as Delfly and the DiLeo et. al. dragonfly-inspired robot [1], [2], to the piezoelectric actuator driven Berkeley Micromechanical Flying Insect (MFI) and Harvard Fly [3], [4], and as size scale decreases, it becomes more difficult to find a balance. The Harvard Fly, composed of a single piezoelectric actuator driving two wings, has displayed the ability to lift its own weight, traveling vertically along guide wires, but cannot yet be controlled in free flight [4]. The Berkeley MFI has four actuators allowing independent control of wing leading and trailing edges and can be controlled in hover in simulation [3], but has not yet demonstrated liftoff.

This work presents an analysis on an attempted compromise between system complexity and final vehicle

L. L. Hines, is with the Robotics Institute, Carnegie Mellon University, Pittsburgh, PA 15213 USA; (e-mail: lhines@cmu.edu).

V. Arabagi, is with the Mechanical Engineering Department, Carnegie Mellon University; (e-mail: varabagi@andrew.cmu.edu).

M. Sitti is with the Mechanical Engineering Department and Robotics Institute, Carnegie Mellon University; (phone: 412-268-3632; e-mail: sitti@cmu.edu).

control based on the passive wing rotation based MAV platform presented in [5]. Four designs, with various means of producing pitch and roll body torques, are examined to verify that a feasible balance has been reached. The consequences of each design choice, with differences in mass, potential delay of utilized smart materials, and lift nonlinearities, are examined in their performance under an LQR controller. Each design's performance in tracking different trajectories is simulated and evaluated.

II. SYSTEM MODELING

A. General System Description

Each design variation is based upon a carbon fiber body housing piezoelectric actuator(s), a spherical four-bar transmission, and a passively rotating wing. Conceptual designs can be seen in Fig. 1. The leading edge of the wing is driven by the actuator while the trailing edge is allowed to passively rotate as affected by wing flexure stiffness, damping, and aerodynamic forces (see Fig. 3). As the trailing edge cannot be directly controlled, mean lift production can be varied by changing actuator amplitude, frequency, and, if one includes a variable stiffness wing hinge, wing flexure stiffness. Asymmetrical wing trajectories, however, cannot be produced, leaving vehicle yaw not directly controllable.
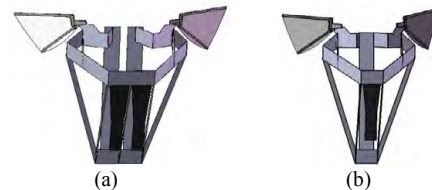

Fig. 1. Conceptual design of a two (a) and one actuator (b) MAV.

Pitch and roll can be induced by varying the lift force between each wing and shifting the center of gravity or center of lift, respectively. Center of lift shifting can be accomplished by changing the voltage bias of the driving actuator, as suggested in [6]. As the system is underactuated and strict limits exist on the forces and torques the wings can produce, the designs will not be able to approach the high maneuverability of a fly, however, with control of mean lift, roll, and pitch, it is not unreasonable to expect the system to be able to reach each translational position in 3D space.

B. Dynamic Model

The dynamic model of the MAV is based on a simplified lumped mass model, as seen in Fig. 2.
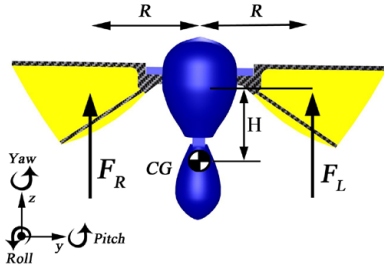
Fig. 2. Vehicle free body diagram.

Newton's equations of motion in the vehicle body frame are as follows:

$$m(\dot{\vec{v}} + \vec{\omega} \times \vec{v}) = \sum_n \vec{F_n} \tag{2}$$

$$J(\dot{\vec{\omega}} + \vec{\omega} \times J\vec{\omega}) = \sum_n \vec{M_n} \tag{3}$$

where $\vec{F}$ and $\vec{M}$ are the forces and moments on the body, $\vec{v}$ and $\vec{\omega}$ are translational and angular velocity, and m and J are body mass and inertia matrix, respectively. The inertia matrix is assumed to be diagonal because of the proposed body shape, which will have insignificant non-diagonal terms. The external forces in the body reference frame, (4)-(9), include the force of gravity, viscous damping, and left and right wing lift forces.

$$F_x = -mG_x - bv_x^2 \tag{4}$$

$$F_y = -mG_y - bv_y^2 \tag{5}$$

$$F_z = -mG_z - bv_z^2 + (F_L + F_R) \tag{6}$$

$$M_x = (-F_L + F_R)R \tag{7}$$

$$M_y = (F_L + F_R)U_3 \tag{8}$$

$$M_z = 0 \tag{9}$$

The vector $\vec{G} = [G_x\ G_y\ G_z]$ is the force of gravity expressed in the body coordinate frame. The constants R and H are shown in Fig.2 and are 1.5 cm and 2.5 cm, respectively. The variable b represents the coefficient of viscous friction and is estimated using frontal surface area to be 0.0114 kg/m. The inputs to the system are F_L, F_R, and U_3. The variables F_L and F_R denote the lift forces produced by the left and right wing, respectively, while U_3 represents the distance in the x direction the center of gravity, or wing center of lift, has been shifted.

C. Lift Force Modeling

The theoretical model of wing lift force generation is formulated from three components: the actuator quasi-steady dynamics, four-bar transmission kinematics, wing dynamics, and quasi-steady aerodynamic forces. The piezoelectric bimorph bending actuator, composed of two layers of carbon fiber and two layers of PZT-5H, has been modeled alike presented in [7] to yield tip displacements (Δ) and force output as a function of input voltage. In order to centralize the mass of the system, the actuator needs to be mounted normal to the wing stroke plane, leading to the design of the spherical four-bar, portrayed in Fig.3. Since the four-bar

links are considered massless, only the kinematic motion and force transmission equations have been considered for the transmission. Furthermore, as the wing is attached to the γ link via a flexure acting as a spring/damper, its flapping angle θ is driven by the actuator, while its rotation is determined by the rotational spring torques and small Reynolds number aerodynamic forces acting on the wing through its motion. Thus the complete theoretical model is able to predict wing lift and drag forces based on the input signal into the actuator. Mathematical modeling details can be found in [5]. Four-bar link lengths used are $[\alpha, \beta, \gamma] = [35, 14, 6]$ mm, with an actuator connection point of 5.5 mm from the α link rotational axis. Total wing length is 27 mm with a maximum chord length of 14 mm.
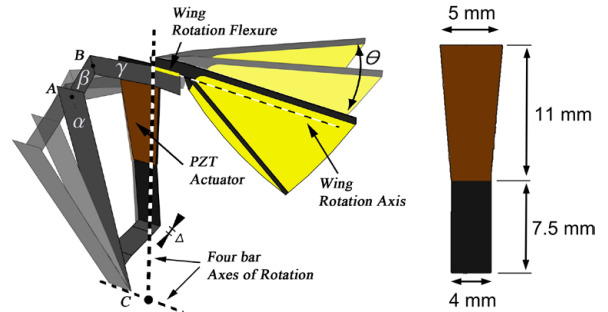

Fig. 3. Schematic of the spherical four-bar, actuator, and wing system as well as actuator dimensions. Points A and B move in trajectories on the surface of an imaginary sphere centered at C.

The mean lift calculated for the chosen four-bar, actuator, and wing dimensions is shown in Figures 4 and 5. Figure 5 is a cross section of the lift surface in Fig. 4, showing change in lift with change in amplitude for a wing flexure stiffness of 19 mN.mm.
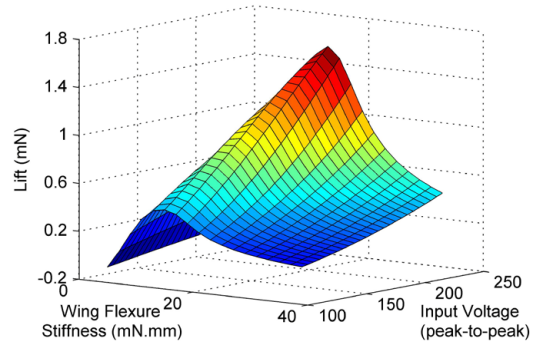

Fig. 4. Mean lift surface given system input peak-to-peak voltage and wing flexure stiffness. System simulation was run at 55 Hz.
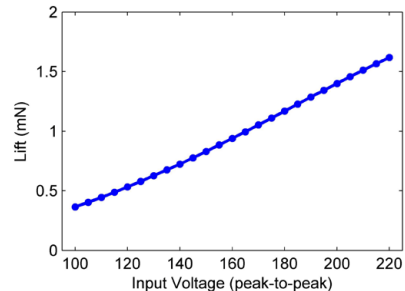

Fig. 5. Mean lift curve due to changing input peak-to-peak voltage. Points indicate calculated values. System simulation was run at 55 Hz and 19 mN.mm wing flexure stiffness.

D. Proposed Design Variations

Each of the proposed designs involve a different combination of morphologies for flight control, namely inducing roll with either change in individual wing amplitude or wing flexure stiffness, and inducing pitch with a shift in center of lift or center of gravity. Each design is summarized in Table 1, below.

TABLE 1
DESIGN VARIATIONS

Design	Lift	Roll	Pitch
Plant 1	Wing amplitude	Individual wing amplitude change	Center of gravity shifting
Plant 2	Wing amplitude	Individual wing amplitude change	Wing center of lift shifting
Plant 3	Wing amplitude (coupled) and wing flexure stiffness	Individual wing flexure stiffness change	Center of gravity shifting
Plant 4	Wing amplitude (coupled) and wing flexure stiffness	Individual wing flexure stiffness change	Wing center of lift shifting

While varying wing frequency will also produce a change in lift, the change is nonlinear. Due to this, and the efficiency advantages of running the system at resonance, the frequency is set as a constant 55 Hz between systems. Figures 4 and 5 depict the lift surface relevant to plants 1, 2 and plants 3, 4 respectively. Figure 6 demonstrates the alternatives in producing a pitch and roll moment.
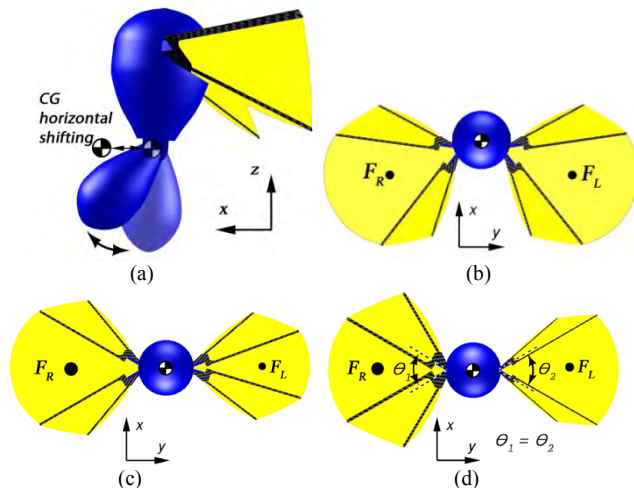

Fig.6. (a,b): Means of inducing a pitch moment, with center of gravity and center of lift shifting, respectively. (c,d): Means to produce a roll moment with asymmetric wing forces. In (a), the center of gravity (CG) is assumed to be moved strictly horizontally for simplicity of calculations. Figure (c) shows a difference in wing amplitudes which occurs in plant 1 and plant 2. Figure (d) shows differing wing rotation magnitudes produced by varying wing flexure stiffness.

It is not readily apparent which design is the best choice. A two actuator system is potentially more maneuverable in roll, has a linear change in lift with change in input voltage amplitude, but has greater mass due to the addition of another piezoelectric actuator. A single actuator system is lighter, but relies upon changing the stiffness of the wing flexure to induce roll, since wing stroke is coupled. A smart material could be used to change wing flexure stiffness, but depending on the material chosen, a delay could be introduced to the system, making control difficult or impossible. Shifting the wing center of lift is restricted by the failure limits of the driving actuator and is dependant on the transmission, but can be changed almost instantaneously. By implementing center of gravity (CG) shifting, with a material with a high strain rate, a greater torque can be produced on the body, but once again, at the cost of introduced delay.

The varying system configurations rely on different morphologies, which are reflected in each design's system parameters. In plants 1 and 2, two actuators are needed to drive the wings at different amplitudes, increasing total system mass. Plants 3 and 4 need only one driving actuator, but rely upon a change in wing flexure stiffness to produce varying wing lift force. The hypothetical system weight is driven primarily by the number of piezoelectric actuators, keeping the carbon fiber frame between systems constant. Table 2 contains the parameters used for each plant. The carbon fiber body and nominal additional mass is set to 100 mg, while the simulated piezoelectric actuator is estimated as 70 mg.

TABLE 2
VARIED SYSTEM PARAMETERS

Design	Actuator Number	Mass, m	Inertia, $J=[J_x, J_y, J_z]$
Plant 1,2	2	240 mg	[25.4 24.1 7.0] g mm^2
Plant 3,4	1	170 mg	[20.2 19.1 5.6] g mm^2

The parameters R, the lift force moment arm, and H, the vertical distance between the center of gravity and center of lift, depicted in Fig. 2, are assumed to remain constant between design variations.

There are limits imposed on the control inputs in each case. The piezoelectric ceramic is prone to fracture at high displacements and high force, which limits the maximum input voltage amplitude that can be applied to the system. Actuator stress, calculated conjointly with lift, approaches 50 MPa at 220 Vpp, which is set as the practical limit. This bound is not unreasonable, given the PZT-5H failure stress determined by experiment to be 61.5 MPa [8] and observed to be a considerably greater 200 MPa [7].

Shifting the wing center of lift is limited by the driving actuator depoling voltage and the induced stress on the actuator. PZT-5H has a depoling voltage of about -40V; applying a higher magnitude negative voltage could result in a degradation of the piezoceramic polarization, which would affect actuator performance. To allow bias shifting, we operate at a nominal offset of 60 V_{DC}, allowing a bias change of +/- 100 V. With the current four-bar design, this results in a limited +/- 5 mm shift of center of lift.

Other bounds on the control inputs are more arbitrary. The limits of CG shifting are set to be +/- 1cm, being greater than the center of lift shifting, since it is more dependent on the actuator chosen. The lower bound on input voltage amplitude and the upper bound for wing flexure stiffness are

chosen at values where lift is about half of what is required for liftoff.

There are several uncertainties with the system definitions, which can be expected in the initial stage of design, rendering co-design of morphology and control more difficult. Implementation of any of these designs would begin with tethered flight, which would allow the majority of additional mass to be placed off-board; an additional unknown mass, electronics, power supply, etc., would be necessary for free powered flight. Optimization of the actuator and transmission has not yet been completed, where a final design could help compensate for inaccurate estimations of required mass.

For lift production estimation, each system is assumed to use the same spherical four-bar mechanism model. This assumption implies that a single actuator driving two wings will have the same performance as an actuator driving only one. In actuality, the single actuator system would need an enlarged actuator to produce similar performance, but total actuator mass, and accompanying carbon fiber and other support would remain significantly less.

III. SIMULATIONS

A. Assumptions

The full system simulation includes body dynamics as discussed above, but relies on a pre-calculated lift map to determine wing forces. Mean lift is calculated offline for given control inputs within the defined bounds. While wing lift and drag forces are time variant, the periodic forces occur at a high frequency, and the simulation is run with a time invariant model driven by the average wing force over a full wing stoke. Wing drag remains symmetrical throughout a wing stroke due to the passive nature of the wing and changes primarily only in magnitude as mean lift force increases.

Simulations were run both with and without a sensor model. The plots included in this paper are system results without considering the sensor model, with the assumption that all states are observable and noise free. Results including the sensor model, based on an accelerometer and gyroscope with performance comparable to existing MEMS sensors available from Colibrys and Sensonor (0.1 mg/min random bias drift and 75 deg/h null error, respectively), produced the same performance trend between plants. The results without the sensor model were chosen to be depicted as the inherent randomness of the model make a direct comparison between individual simulation runs difficult.

B. Control Scheme

At the beginning of each wing stroke, the system is linearized and the ideal LQR gain matrix is calculated [9]. The LQR gain matrix is used to find the control input, which remains constant over the wing stroke. The state weights for LQR were chosen as appropriate for the desired trajectory with translational position emphasized. Due to the underactuated nature of system, many trajectories are physically impossible to follow exactly. To compensate for this and the fact that it is difficult to determine the required pitch and roll angles in each case, desired roll and pitch angles were set to zero, encouraging a stable configuration. Control weights remained constant between plants (diagonal matrix with elements of value 100), and control inputs for each plant were scaled with their defined bounds to remain within a range of [0, 1].

C. Results

Each plant is simulated following three different trajectory types: 1) straight line motion in the XY plane, 2) circles in the XY plane, and 3) selected edges of a cube. In addition, each trajectory is repeated with a control delay on the proposed inputs, a likely side effect of using a smart material. These delays correspond to 1, 2, and 3 wing strokes at approximately 18, 36, and 54 msec.

In trajectory set 1, each modeled plant is asked to follow a series of straight paths along different angles in the XY plane, as depicted in Fig. 7(b). LQR state weights were set to 100 for x, y position, 10 for x, y velocity, and 1 otherwise. The desired trajectories of length 50 cm were to be completed in 5 seconds. Note that as yaw is not directly controlled, the robot yaw orientation stays approximately constant throughout all trajectories.
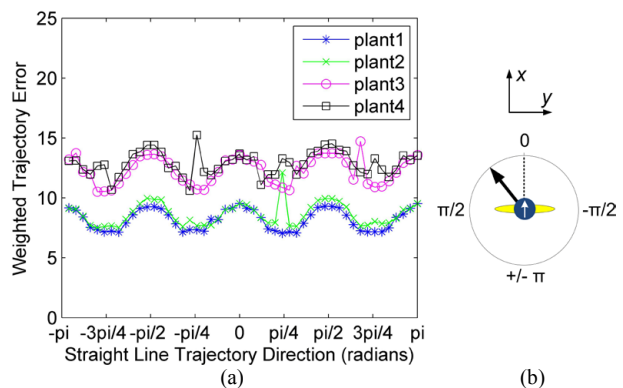

Fig. 7. (a) Weighted trajectory error for straight line trajectories in the XY plane in systems with zero delay. A distance of 50 cm was to be covered in 5 seconds. (b) Depiction of desired trajectories in XY plane.

The weighted error for each trajectory is plotted over the trajectory direction in Fig. 7. The error was weighted with the state weights chosen for LQR. The difference in cost between traveling in only the X or Y direction versus traveling diagonally is in part due to the desired velocity. Higher roll and pitch angles are more difficult to reach and maintain. In diagonal motions, a smaller individual roll and pitch angles are needed to reach the same total velocity as motions requiring only a pitch or roll angle deviation. Since desired roll and pitch angles are set to zero, the difference in required and actual roll and pitch angles for various trajectories could contribute to the error variation in Fig. 7, but on average their total weighted error varied less than 0.5, and cannot be the sole source of this effect.

The weighted error given each trajectory and delay can be seen in Fig. 8. Plant 2 is excluded as it does not incorporate any materials with potential delays. In both plant 1 and 3, the controller fails with a delay of 54 msec, suggesting that

any smart material with a slower response time, in at least in regards to center of gravity shifting, would be a poor choice. Smaller time delays across plants resulted in comparable performance to the no delay case.
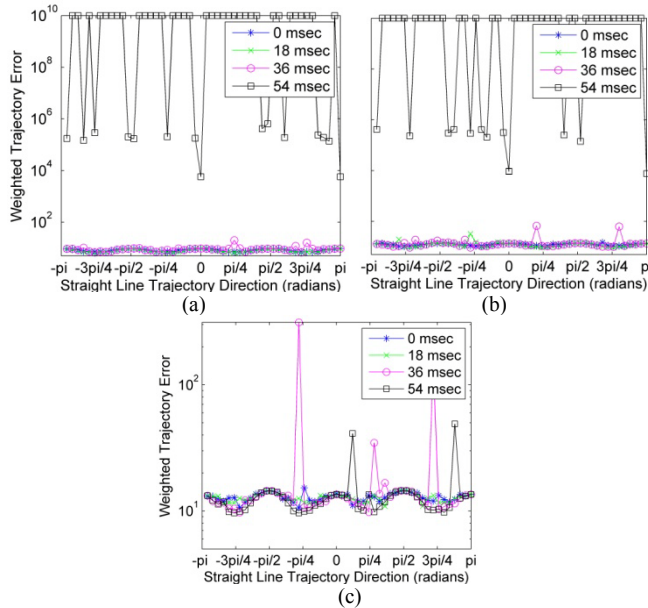

Fig. 8. Weighted trajectory error for straight line trajectories in the XY plane. Plots (a)-(c) are plants 1, 3, and 4 respectively. Weighted error values of 10^{10} denote divergence.

The second trajectory set is composed of a series of circles with increasing radius to be completed in 5 seconds, an example of which is portrayed in Fig. 9. LQR state weights were set to 100 for x, y position, 10 for x, y velocity, and 1 otherwise.
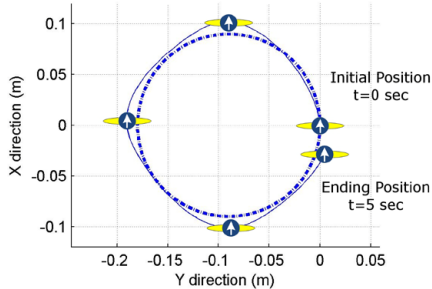

Fig. 9. Example performance in trajectory following. Simulation run with plant 4 on a circle with radius of 9 cm. Dotted line is desired XY position, continuous line is actual position.

The weighted trajectory error for circles of increasing radius can be seen in Fig. 10. Performance between plants remains similar up to a circle of radius 15 cm, after which performance is inconsistent due to greater desired body velocities. The trajectories repeated with control input delays are depicted in Fig. 11. As with the straight line trajectories, delays of 56 msec show failure in plants 1 and 3. While at lower trajectory velocities plant 4 can handle the delay, as body velocity increases, all plants are more susceptible to control input delays and experience failure at circles with a radius of 30 cm.

The third trajectory set is composed of smoothed paths along the edges of a cube with varying edge lengths, an example of which can be seen in Fig. 12. LQR state weights

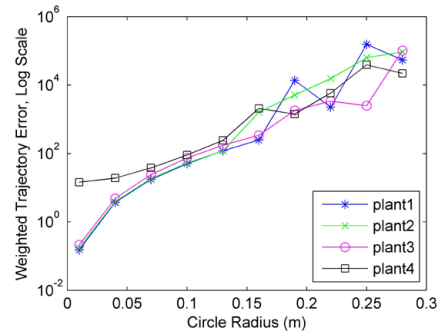were set to 100 for x, y, z position, 10 for x, y, z velocity, and 1 otherwise.

Fig. 10. Weighted trajectory error for circle trajectories in the XY plane in systems with zero delay.
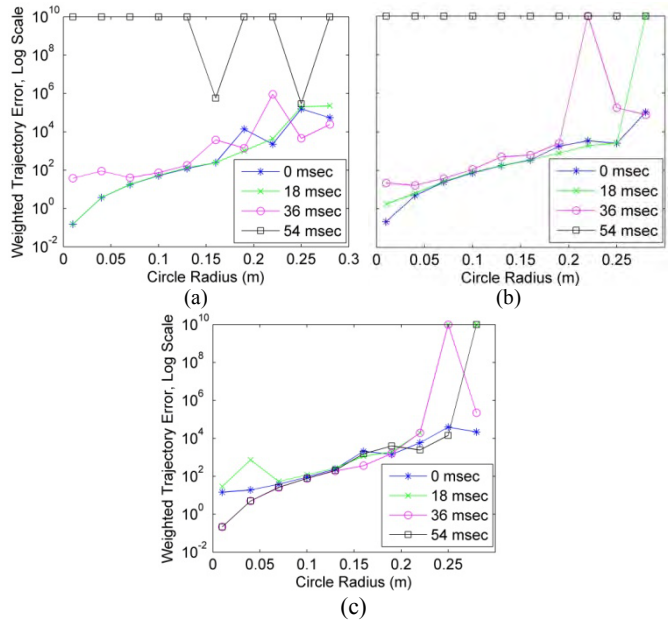

Fig. 11. Weighted trajectory error, log scale, for circle trajectories in the XY plane. Plots are, in order from (a)-(c), plants 1, 3, and 4. Weighted error values of 10^{10} denote divergence.
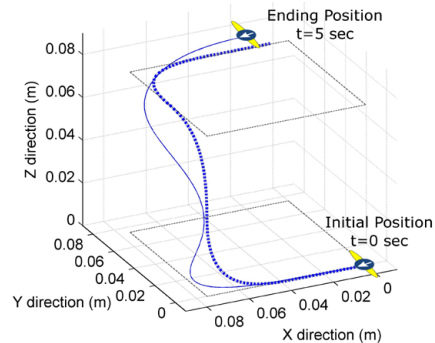

Fig. 12. Example performance in 3D trajectory following. Simulation run with plant 4 on a cube with edge length of 7 cm. Dark blue dotted line is desired position, continuous light blue line is actual position.

Performance over increasing cube sizes, with no delay, is depicted in Fig. 13 while simulation results with control input delays can be seen in Fig. 14.

Unlike the circle trajectories, neither plant 1 nor plant 3 can handle the lowest tested control input delay. Plant 4's performance is similar between 0 and 18 msec delays, but

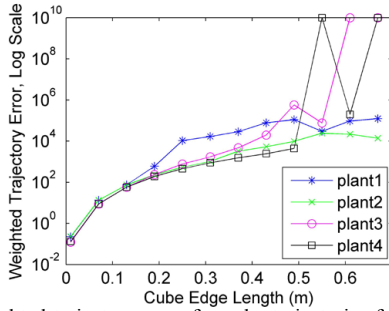also experiences performance degradation at delays of 36 and 54 msec.

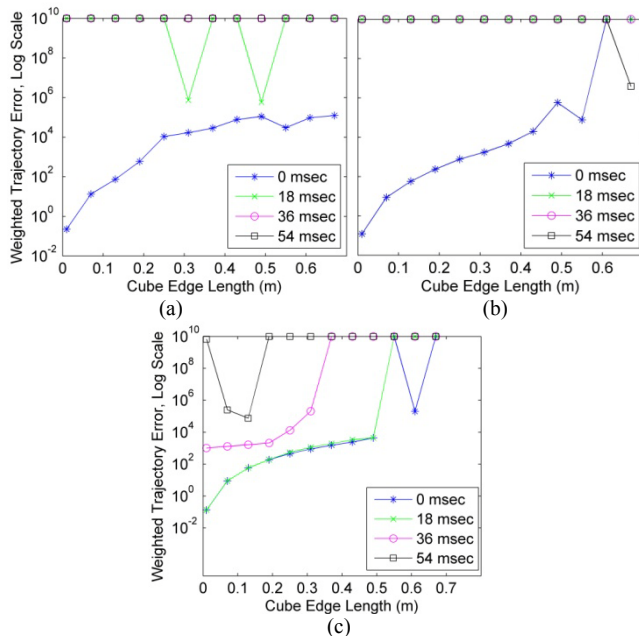Fig. 13. Weighted trajectory error for cube trajectories for systems with zero delay.

Fig. 14. Weighted trajectory error, log scale, for cube trajectories. Plots are, in order from (a)-(c), plants 1, 3, and 4. Weighted error values of 10^{10} denote divergence.

IV. DISCUSSION AND CONCLUSION

In this work, several possible design variations for a flapping wing based MAV were compared given their performance under an LQR controller. Overall, LQR produced reasonable results even given the system nonlinearities and small control input delays.

Across trajectories there is little practical difference between the center of gravity and wing bias shifting in zero delay systems, which is reassuring given the restrictions in the single actuator systems. Performance is more closely grouped by the number of piezoelectric actuators and even then remains similar across plants. Delay, given implemented via smart materials, is the greatest concern to all control scenarios. For delays of less than 54 msec, system performance remains similar across plants in both straight line and circle trajectories. Plant 4, however, has shown better resistance to the applied control input delays overall, experiencing controller failure in fewer instances.

At 54 msec, however, performance degrades considerably

at even low system velocities. This restricts the possible smart material choices significantly, although it does not make the implementation of such actuators unfeasible. Ionic Polymer-Metal Composites, which have a higher strain rate and are less dense than piezoelectrics, have a response time of as little as 10 msec depending on their construction.

While the success of any of these design alternatives is not assured, the simulation results can help direct continued design development. Of the possible design choices, plant 2, with two actuators and center of lift shifting, would be the simplest to implement, though plant 4's performance shows it a possible alternative. Center of lift shifting has no additional cost of implementation with either single or double actuator design and manufacturing a two actuator system would be less difficult than incorporating a smart material for variable wing flexure stiffness. Relevant to the current design variations, possible problems that would need to be addressed include unintended amplitude coupling between wings due to body vibrations, and alignment of the two actuator-transmission systems during assembly. As wing center of lift is severely limited in its motion, misalignment between the center of mass and wings could make pitch control impossible.

Future work includes continuing design development, consisting of optimizing the spherical four-bar transmission for lift production, designing a thoracic frame, etc. After a prototype has been developed, the approach of using of a linear controller can be first tested on a restricted degree of freedom platform, uncoupling and controlling pitch and roll control individually. One assumption from the control perspective that should be confirmed is the impact of time variant forces in the model, although LQR has been demonstrated successfully on a similar system in [3].

REFERENCES

[1] G. C. H. E. de Croon, K. M. E. de Clerq, R. Ruijsink., B. Remes, and C. de Wagter, "Design, aerodynamics, and vision-based control of the DelFly" *International Journal on Micro Air Vehicles*, vol. 1, no. 2, pp. 71 – 97, 2009.

[2] C. Dileo, and X. Deng, "Design of and Experiments on a Dragonfly-Inspired Robot." *Advanced Robotics*, vol. 23, no. 7-8, pp. 1003-1021, 2009.

[3] X. Deng, L. Schenato, W. Wu, and S. Sastry, "Flapping Flight for Biomimetic Robotic Insects: Part II- Flight Control Design." *IEEE Trans. on Robotics*, vol. 22, no. 4, August 2006.

[4] R. J. Wood, "The first takeoff of a biologically-inspired at-scale robotic insect." *IEEE Trans. on Robotics*, vol. 24, no. 2, pp. 341-347, April, 2008.

[5] V. Arabagi and M. Sitti. "Simulation and analysis of a passive pitch reversal flapping wing mechanism for an aerial platform." *Proceedings of International Conference on Intelligent Robotics and Systems*, pp. 1260-1265, 2008.

[6] B. M. Finio, B. Eum, C. Oland, and R. J. Wood, "Asymmetric flapping for a robotic fly using a hybrid power-control actuator." *Proceedings of International Conference on Intelligent Robotics and Systems*, pp. 2755-2762, 2009.

[7] R. J. Wood, E. Steltz, and R. S. Fearing. "Optimal energy density piezoelectric bending actuators." *Sensors and Actuators*, vol. 119, pp.476-488, 2005.

[8] M. W. Hooker, "Properties of PZT-based piezoelectric ceramics between -150 and 250C." *NASA contractor report*, 1998.

[9] R. F. Stengel, *Optimal Control and Estimation*. Mineola, NY: Dover Publications, 1986.